Adaptive optics enables multimode 3D super-resolution microscopy via remote focusing: Supporting information

Vytautas Navikas[1], Adrien C. Descloux[1], Kristin S. Grussmayer [1,2], Sanjin Marion[1], Aleksandra Radenovic[1]

[1] Laboratory of Nanoscale Biology, Institute of Bioengineering, School of Engineering, Swiss Federal Institute of Technology Lausanne (EPFL), Lausanne, Switzerland. [2] Current address: Grussmayer Lab, Department of Bionanoscience, Faculty of Applied Science and Kavli Institute for Nanoscience Delft, Delft University of Technology, Delft, Netherlands.

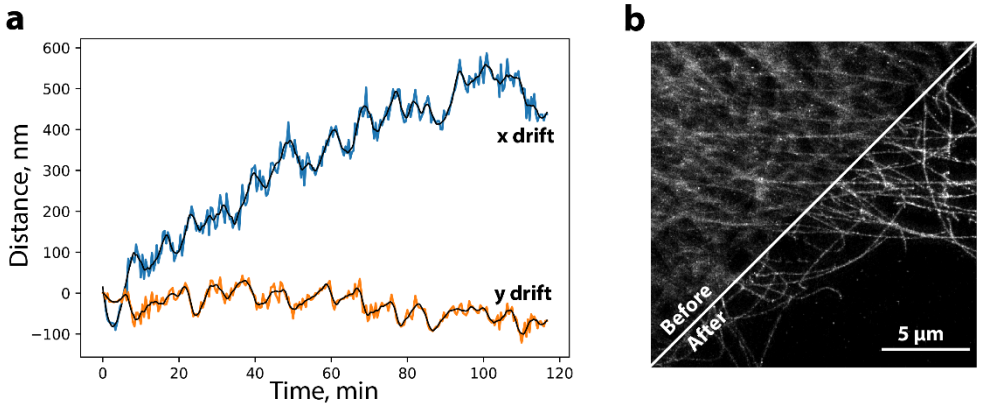

Supporting figure 1. Lateral drift correction with fiducial markers. (a) Lateral x (blue) and y (orange) drift over a total imaging time of 2h. Black lines represent the smoothed signal with a smoothing window of 4.1 min. The smoothed signal was used for correction. **(b)** Max projection of 3D SMLM stack before and after drift correction, showing the apparent visual improvement.

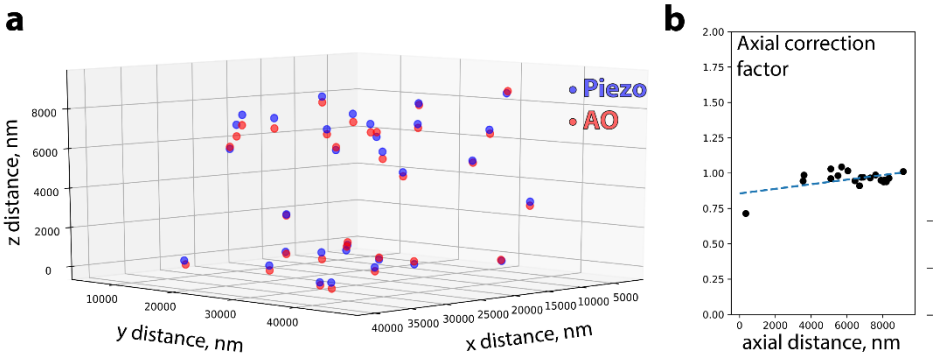

Supporting figure 2. Axial calibration with fluorescent beads. (a) Cumulative 3D localizations from multiple fields of view. The bead sample for axial calibration was prepared in 1% agarose. The beads covered the surface of the coverslip, which was used to align different ROIs axially. The bead stacks were acquired with a piezo stage and by using adaptive optics by adding a constant amount of focus mode. The centers of the beads were subsequently localized in 3D for each ROI (N=6) and the position of the bottom bead was subtracted. Finally, the nearest neighbor for each bead was found between 2 stacks (piezo and AO) and the difference in axial position. **(b)** Axial calibration factor (blue line) used to correct axial positions for each plane.

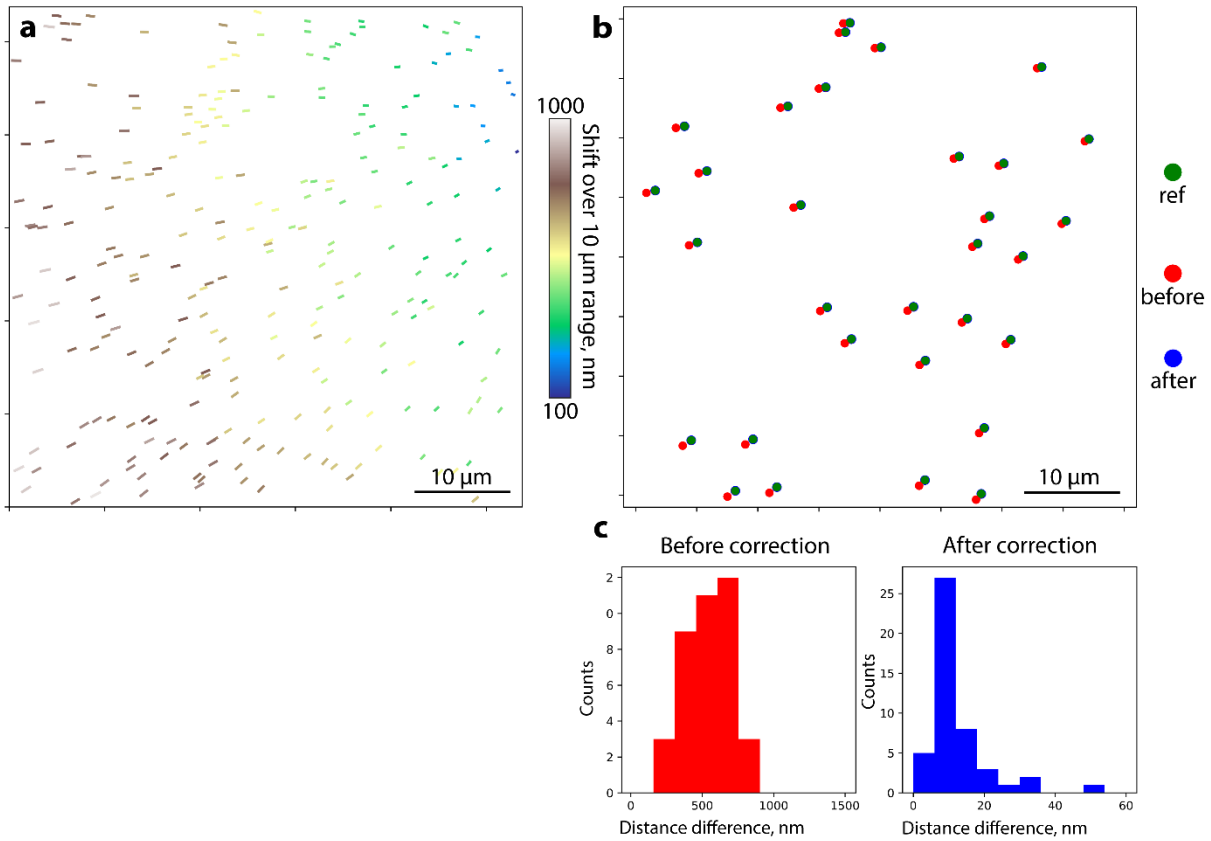

Supporting figure 3. Lateral image distortion correction. SI Figure 3. Correction of the lateral image distortion. To obtain the image transformation matrix we have added a different focus mode values with a deformable mirror (0, 2 µm, 4 µm, …, 10 µm) and refocused the sample with a motorized stage to obtain the image stack with 6 different heights. The bead sample was imaged allowed us to quantify the positions of the beads with the precision far beyond the diffraction limit. An average localization uncertainty of 6.1±1.2 nm was measured. We have found that the remote focus with DM indeed induced the nonlinear deformation over the large (53.76 µm x 53.76 µm) field-of-view (FOV) which was observed as a shift of the bead lateral position (SI Figure 3a). The FOV deformation scaled linearly over the 10 µm focus range and was repeatable over the different samples and for different mirror shapes. We speculate, that this shift is caused by the slight misalignment in the optical system itself. However, the distortion was straightforwardly corrected for each plane using a piecewise affine image transformation, which was able to correct the positions of the beads (lateral positions at 0 µm and 10 µm are compared) with a precision of (12.8±8.6 nm) compared to (541.7±154.8nm) without the correction applied (SI Figures 3b-c).

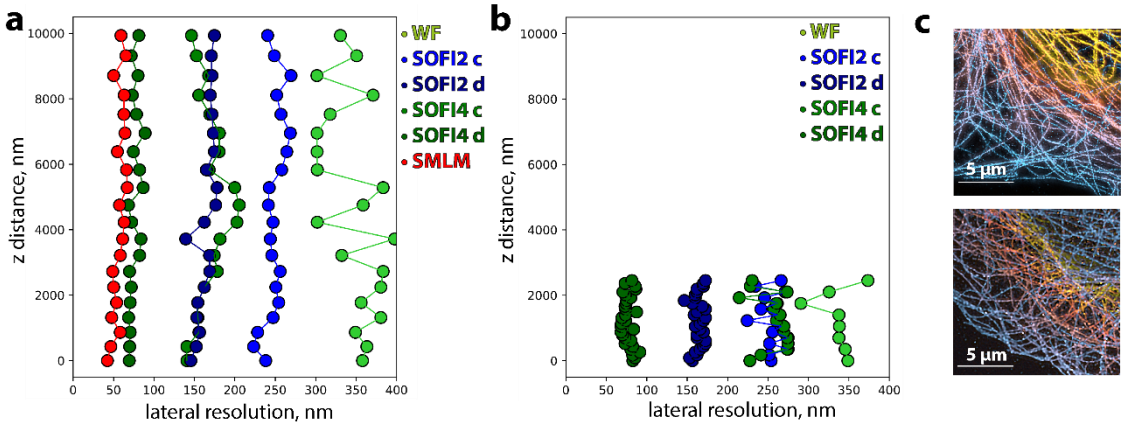

Supporting figure 4. Image resolution comparison. (a) Lateral image resolution per each height plane was estimated with previously published algorithm[2]. Raw SOFI cumulants for 2nd and 4th orders (SOFI2c an SOFI4c) and deconvolved SOFI images for 2nd and 4th orders (SOFI2d an SOFI4d) are shown. Furthermore, resolution was also estimated for SMLM reconstruction from **Figure 3** (SMLM), using bilinear histogram rendering (https://github.com/Ades91/ImDecorr). WF resolution values fluctuate due to a low SNR. **(b)** Corresponding resolution estimates were also done for the 3D SOFI approach published previously[3] using the exact same sample preparation procedure. **(c)** Deconvolved 4th order SOFI images are shown for both imaging approaches (Adaptive optics SOFI 2D – Top) and (3D-SOFI) bottom.

This comparison needs to be interpreted with additional caution and is valid only considering both modalities' intrinsic pros and cons, not just comparing the resolution values directly. Multiplane SOFI imaging was performed with a setup published previously[3,4]. For imaging with adaptive optics, a higher NA objective was used (NA 1.49 compared to NA 1.2), which also contributes to image resolution. On the other hand, an EMCCD camera was used for AO imaging, and an sCMOS for 3D SOFI and it is known that SOFI performs significantly better[5] with sCMOS cameras. Furthermore, the imaging intensity used for 3D SOFI was significantly higher (0.3 W/cm^2 compared to 3.5 W/cm^2). It is also important to note that simultaneous SOFI-3D imaging is significantly faster and allows increased depth sampling by computing inter-plane cross-cumulants, thus providing faster volume acquisition times, however, limited in terms of photobleaching due to the higher laser powers used and it has a fixed Z-range.

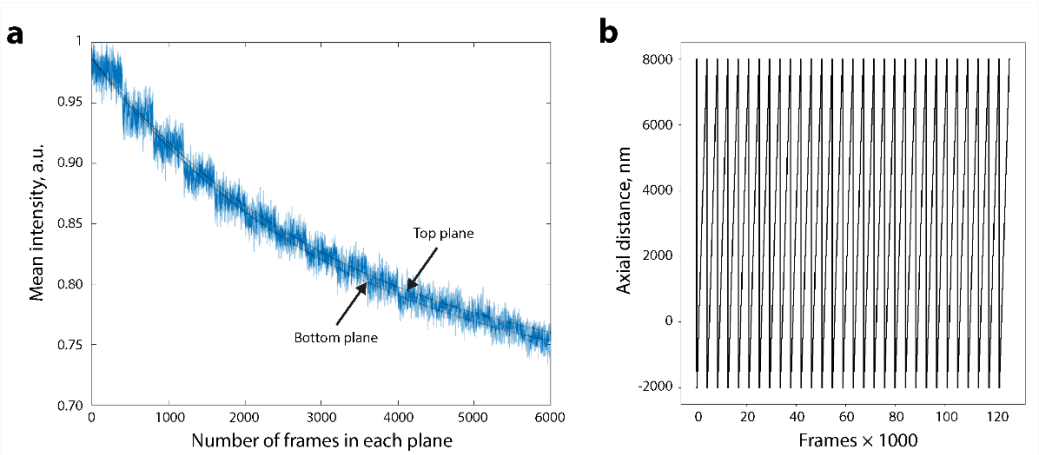

Supporting figure 5. Homogeneous imaging volume bleaching. (a) Bleaching curves for the top and bottom planes spaced 9.9 µm apart. Bleaching lifetimes were estimated by calculating the lifetime for each plane and multiplying by the total number of planes recorded (N=21). The average lifetime was 54.01 ±4.76 min which is due to low laser illumination intensity used (300 W/cm^2) and a degassed PBS buffer used. **(b)** The amount of focus applied with AO over time. The imaging plane was changed every 300 frames (15s) to homogenize the bleaching over the whole image stack.

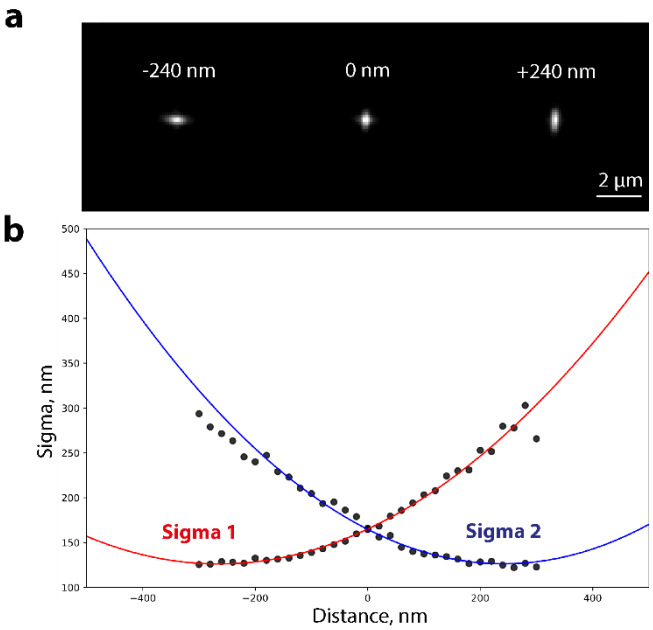

Supporting figure 6. Z-calibration of astigmatic PSF. (a) Bead image at different heights **(b)** PSF's Sigma calibration curve.

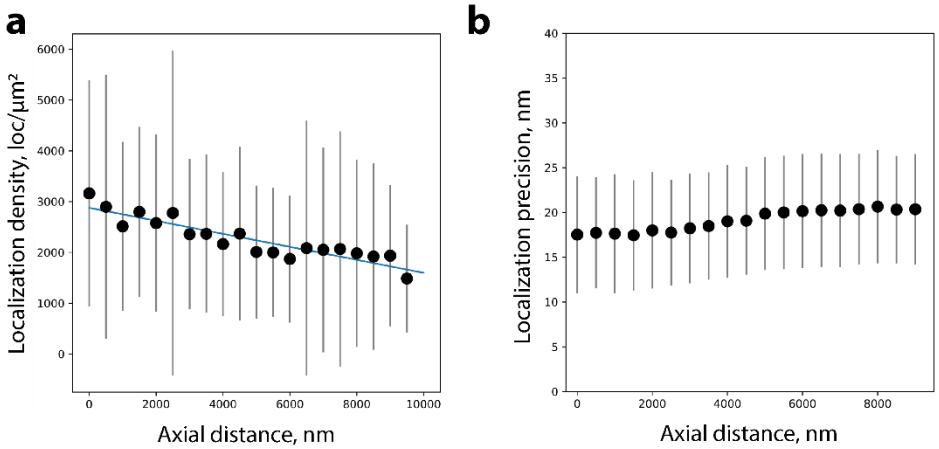

Supporting figure 7. Localization density and localization precision. (a) Localization density for each plane in **Figure 3** displayed as mean±std**.** Localization density was estimated from localization maps with removed duplicate molecules based on localization uncertainty. The data was further thresholded based on density to remove background localizations and the final estimation was done with kNN approach using a KDTree algorithm to get the number of neighbours for each molecule within 20nm search radius. The final value is adjusted for area and mean±std values are plotted. **(b)** Localization precision plot (mean±std) for each image plane in **Figure 3.**

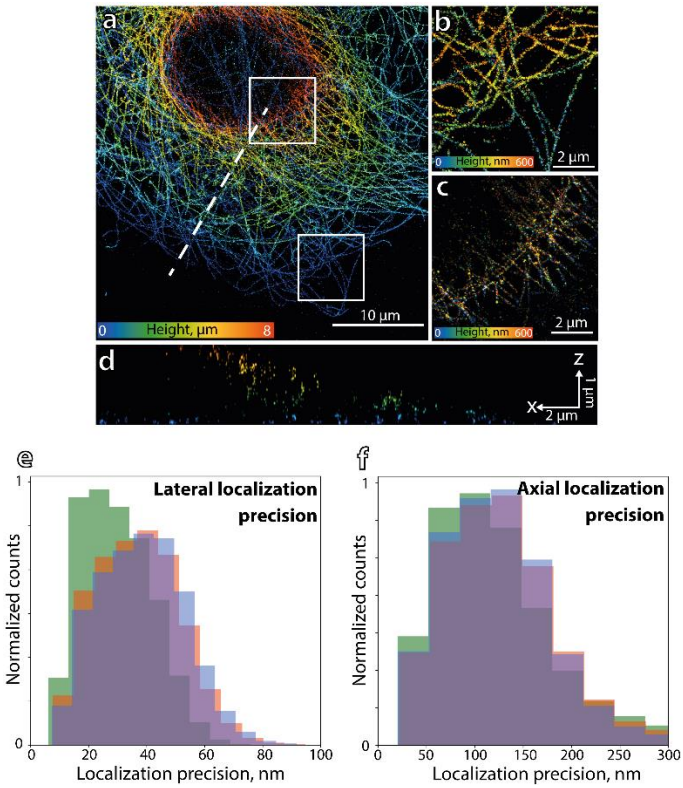

Supporting figure 8. Multiplane astigmatism-based single-molecule localization microscopy with 300nm interplane distance. (a) A height max intensity projection of tubulin in a COS-7 cell immunostained with Abberior FLIP-565 self-blinking dye imaged by adding 60 nm RMS of astigmatism. **(b-c)** Zoom-ins from the bottom **(b)** and top **(c)** planes of the full image stack **(d)** A slice marked in (a) with a dashed line showing the axial profile of the whole volume consisting of 27 sub-volumes spaced with 0.3 µm distance. **(e-f)** Lateral and axial localization precisions estimated with a Thunderstorm routine. The precision values are similar to the previous work[6].

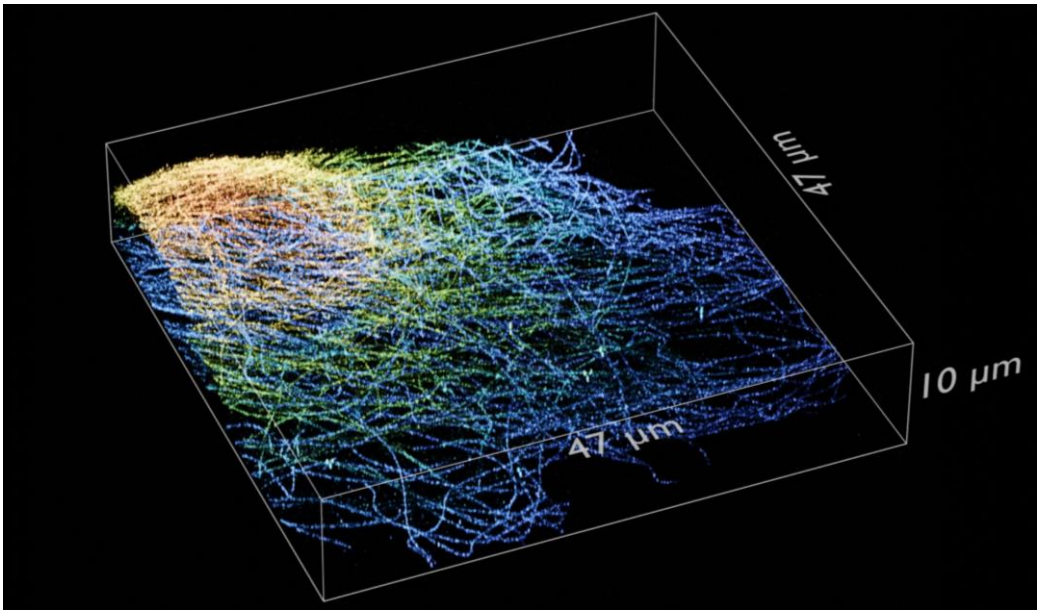

Supporting figure 9. Astigmatism-based 3D SMLM volume. The localized volume was rendered in Blender 3D by using image planes spaced 50nm apart rendered with Thunderstorm[7] plugin. The final rendering was done with cycles rendering engine by using a volumetric rendering functionality.

References

1. Siemons, M. *et al.* Comparing strategies for deep astigmatism-based single-molecule localization microscopy. *Biomed. Opt. Express* **11**, 735 (2020).

2. Descloux, A., Grußmayer, K. S. & Radenovic, A. Parameter-free image resolution estimation based on decorrelation analysis. *Nat. Methods* **16**, 918–924 (2019).

3. Grußmayer, K., Lukes, T., Lasser, T. & Radenovic, A. Self-Blinking Dyes Unlock High-Order and Multiplane Super-Resolution Optical Fluctuation Imaging. *ACS Nano* **14**, 9156–9165 (2020).

4. Descloux, A. *et al.* Combined multi-plane phase retrieval and super-resolution optical fluctuation imaging for 4D cell microscopy. *Nat. Photonics* **12**, 165–172 (2018).

5. Chen, X. *et al.* Superior performance with sCMOS over EMCCD in super-resolution optical fluctuation imaging. *J. Biomed. Opt.* **21**, 066007 (2016).

6. Galland, R. *et al.* 3D high-and super-resolution imaging using single-objective SPIM. *Nat. Methods* **12**, 641–644 (2015).

7. Ovesný, M., Křížek, P., Borkovec, J., Svindrych, Z. & Hagen, G. M. ThunderSTORM: a comprehensive ImageJ plug-in for PALM and STORM data analysis and super-resolution imaging. *Bioinformatics* **30**, 2389–90 (2014).